# Macro- and micro-structure designs for porous sound absorbers

Keith Attenborough, keith.attenborough@open.ac.uk
Engineering and Innovation, The Open University, Milton Keynes, MK7 6AA, UK

**Abstract**

Macro-structures that improve the sound absorption of hard-backed layers of rigid-porous material include graduated arrangements for obtaining impedance matching and vertical and horizontal partitioning which can result in meta-material behaviour. Instead of using bulk-manufactured porous materials as the host media, normal incidence absorption coefficient spectra are predicted for combinations of these macro-structures with simple micro-structures consisting of uniform or non-uniform slits either normal or inclined to the layer surface. The results suggest that, subject to manufacturing constraints, the production of composite structures like these instead of traditional porous sound absorbing configurations would result in comparable or superior acoustical performances.

**Keywords**: porous absorber, slit microstructures, impedance matching, partitions

## 1 INTRODUCTION

An important goal when designing sound absorbing treatments for use in aircraft and vehicle structures, white goods and prefabricated building constructions, is to provide good low frequency absorption while adding as little in volume and weight as possible. Frequently absorption is provided by hard-backed layers of a bulk-manufactured porous material such as glass wool or polymer foam. For harsh environments, metallic fibre materials and foams made, for example, by fusing metal spheres together and then perforating the fused sphere assemblies, are of interest because of their rigidity, lightness and thermal conductivity [1]. Hard-backed thin porous layers have an absorption peak at their quarter wavelength layer resonance. The lower the desired frequency of the peak absorption, the thicker the layer that is required. A classical way of improving absorption is to insert an airgap between the material layer and its rigid backing but this may not be acceptable if space is limited. Alternatives include impedance matching [2], partitioning [3,4] and periodically-spaced inclusions which introduce additional scattering and dissipation mechanisms [5,6].

In previous research on impedance matching, partitioning and inclusions, polymer or metallic foams have been considered to be the host porous media. The pore structures in these materials are complicated, and so is the associated prediction of acoustical properties. A periodic unit cell in the shape of a tetrakaidekahedron, with holed membranes in some of its faces, has been used to study the relationship of microstructure to the acoustical behaviour of polymer foams [7]. This idealised geometry is used with numerical methods such as FEM to deduce the parameters required for semi-analytical models and hence predict the acoustical performance. Of the eight parameters required by in the Johnson-Champoux-Allard-Lafarge-Pride (JCALP) model [8], viz. porosity, air permeability, tortuosity (high frequency limit), thermal permeability, viscous and thermal characteristic lengths, thermal tortuosity and a low frequency tortuosity, the viscous characteristic length, thermal tortuosity and low frequency tortuosity are difficult to measure independently. Considerable efforts have been made to relate such parameters to pore structure, thereby, improving understanding of the influence of pore structure on acoustical performance [7] and of what to control during the manufacturing process [9]. On the other hand, simple pore structures are predicted to yield absorption spectra comparable with, or, indeed, better than those achieved with bulk manufactured materials [10].

Previously the acoustical performances of rigid-framed media containing identical uniform pores inclined to the surface, sinusoidally-sided slits, annular cylindrical pores and slit arrays

with two significantly-different cross sections (dual porosity) have been considered separately and in combination [10]. These pore structures increase tortuosity thereby increasing the effective path length and reducing the sound speed through the hard-backed layer. The result is a lowering of the frequency of the quarter wavelength layer resonance without increasing the layer thickness. An alternative approach, not pursued here, is to increase the effective compressibility in a porous medium, for example, by using narrow cylindrical dead-end pores as side branches to main pores [11].

Additive manufacture of sound absorbers with simple pore structures has been investigated [12,13]. So far, however, not much use has been made of knowledge about the influence of pore structure on acoustical properties. For example, the changes in absorption observed with pore inclination in perforated samples manufactured by 3D printing [12] are predictable [10]. Moreover, macro-structural effects have not been considered. In principle, subject to the constraints of additive manufacturing processes [14], it should be possible to devise internal structures at macro- and micro-scales that realise any desired sound absorption performance.

After revising a model for the acoustical properties of arrays of parallel, uniform, identical slits, previous work [2-4,10] is extended by predicting the absorption spectra yielded by impedance matching, periodic non-uniformity and partitioning in simple slit-pore structures.

# 2 PARALLEL INCLINED SLITS

## 2.1 Uniform slits

The complex density in a (single) uniform slit may be written [15]

$$\rho(\omega) = \rho_0 / H(\lambda)\,,\; H(\lambda) = 1 - \tanh\left(\lambda\sqrt{-i}\right)/\left(\lambda\sqrt{-i}\right) \tag{1a,b}$$

where $\omega$ is the angular frequency and the dimensionless parameter $\lambda = b\sqrt{(\omega/\nu)}$, $b$ is the semi-width of the slit, $\nu = \mu/\rho_0$ is the ratio of the dynamic coefficient of viscosity to equilibrium air density. $\lambda$ represents the ratio of the slit width to the frequency-dependent thickness of the viscous boundary layer.

The complex compressibility is given by

$$C(\omega) \;=\; (\gamma P_0)^{-1}[\gamma - (\gamma - 1)H(\lambda\sqrt{(N_{PR})})] \tag{2}$$

where $(\gamma P_0)^{-1} = (\rho_0 c_0^2)^{-1}$ is the adiabatic compressibility of air, $c_0$ is the adiabatic sound speed in air and $N_{PR}$ is the Prandtl number.

The (steady) flow resistivity ($R_S$) of an array of slits width $2b$, tortuosity $T$ and porosity $\Omega$ are related by making use of the Kozeny-Carman formula [16],

$$R_s = \frac{3\mu T}{\Omega b^2} \tag{3}$$

If the pores are inclined at angle $\theta$ to the surface normal, then [17]

$$T(\theta) = 1/\cos^2(\theta) \tag{4}$$

The complex density ($\rho_b(\omega)$) and complex compressibility ($C_b(\omega)$) for the bulk material are calculated from those for an individual pore using equations (5a,b):

$$\rho_b(\omega) = (T/\Omega)\rho(\omega),\;\; C_b(\omega) = \Omega C(\omega) \tag{5a,b}$$

The bulk propagation constant ($k(\omega)$) and normalised characteristic impedance ($z_c(\omega)$) of the porous material containing identical parallel slits, of width $2b$ separated by solid strips of width $L = 2b(1 - \Omega)/\Omega$, may be calculated from equations (6a,b).

$$k(\omega) = \omega\sqrt{\rho_b(\omega)C_b(\omega)},\; Z_c(\omega) = (\rho_0 c_0)^{-1}\sqrt{\rho_b(\omega)/C_b(\omega)} \tag{6a,b}$$

The surface impedance of a hard-backed porous layer of thickness $d$ is,

$$Z(d) = Z_c \coth(-ikd) = iZ_c \cot(kd). \quad (7)$$

The plane wave reflection coefficient, $R(d)$, and normal incidence absorption coefficient, $\alpha(d)$, for a hard -backed porous layer are given, respectively, by equations (8a,b):

$$R(d) = \frac{Z(d)-\rho_0 c_0}{Z(d)+\rho_0 c_0}, \qquad \alpha(d) = 1 - \left|\left(R(d)\right)\right|^2 \quad (8,9)$$

## 2.2 Impedance matching

The surface impedance of a hard-backed multiply-layered material is given by the recursion formula [2]

$$Z_s(x_n) = Z_{n-1} \frac{iZ_s(x_{n-1})\cot(k_{n-1}d_{n-1})+Z_{n-1}}{Z_s(x_{n-1})+iZ_{n-1}\cot(k_{n-1}d_{n-1})} \quad (10)$$

where $Z_{n-1}$, $k_{n-1}$ and $d_{n-1}$ are the characteristic impedance, propagation constant and thickness of the (n – 1)$^{th}$ layer respectively. The location of the n$^{th}$ interface is given by $x_n$ and $x_1$ is the surface of the hard backing.

Figure 1(a) compares absorption coefficient spectra predicted for an 45 mm thick hard-backed layer of identical 0.18 mm wide slits inclined at 40° to the surface normal and a 30 mm thick gradient inclined slit configuration consisting of three sub-layers having successively reducing slit widths and widths of solid between adjacent slits and increasing inclinations (see Table 1 in which sub-layers are numbered from the upper surface and the edge-to-edge distances are abbreviated by 'spacing'), with that predicted by the Johnson-Allard-Champoux-Lafarge (JCAL) model for a 57 mm thick melamine foam layer [1]. The JCAL values of porosity ($\Omega$), flow resistivity ($R_s$), tortuosity ($T$), thermal permeability ($\kappa_0$), viscous characteristic length ($\Lambda$) and thermal characteristic length ($\Lambda'$) are listed in Table 2. Sketches of the inclined slit configurations considered are shown in the Figure.

Figure 1(b) compares the absorption coefficient spectrum (solid black line) predicted using the Johnson-Allard-Champoux (JCA) model [1] with parameter values listed in Table 2 for a 26.4 mm thick perforated aluminium foam and the, with those predicted for an 25 mm thick uniform hard-backed layer of identical 0.46 mm wide slits inclined at 65° to the surface normal (dash-dot blue line) and a 26.4 mm gradient inclined slit configuration (broken red line) having three sub-layers with widths, edge-to-edge distances and inclinations listed in Table 1.

**Table 1** Gradient inclined slit system parameters

| | Figure 1(a) | | | | Figure1(b) | | | |
|---|---|---|---|---|---|---|---|---|
| Sub-layer | slit width ($2b$) mm | spacing ($L$) mm | angle ($\theta°$) | thickness mm | slit width ($2b$) mm | spacing ($L$) mm | angle ($\theta°$) | thickness mm |
| 1 | 0.3 | $3\times10^{-3}$ | 60 | 7.5 | 2 | 5.14 | 50 | 4 |
| 2 | 0.2 | $2\times10^{-3}$ | 65 | 10 | 1 | 2.57 | 60 | 8 |
| 3 | 0.1 | $1\times10^{-3}$ | 70 | 12.5 | 0.5 | 1.29 | 70 | 14.4 |

**Table 2** Parameter values used in JCAL model for a melamine foam and the JCA model for a perforated aluminium foam [1]

| Foam/parameter | $\Omega$ | $R_s$ kPa s m$^{-2}$ | $T$ | $\kappa_0$ m$^2$ | $\Lambda$ mm | $\Lambda'$ mm |
|---|---|---|---|---|---|---|
| melamine | 0.99 | 12 | 1.01 | $1.5\times10^{-9}$ | 0.1 | 0.4 |
| aluminium | 0.283 | 8.433 | 3.5 | - | 0.281 | 1.504 |

The uniform inclined slit layer is predicted to yield an absorption comparable with that predicted for a melamine foam layer while being 21% thinner. The gradient slit layer is predicted to offer comparable absorption with a significantly (47%) smaller thickness. In contrast the gradient slit arrangement does not offer clear absorption advantage compared with a low porosity metallic foam example (Fig. 1(b)). But, overall, both uniform inclined slit and gradient slit layers are predicted to offer a slightly greater absorption.

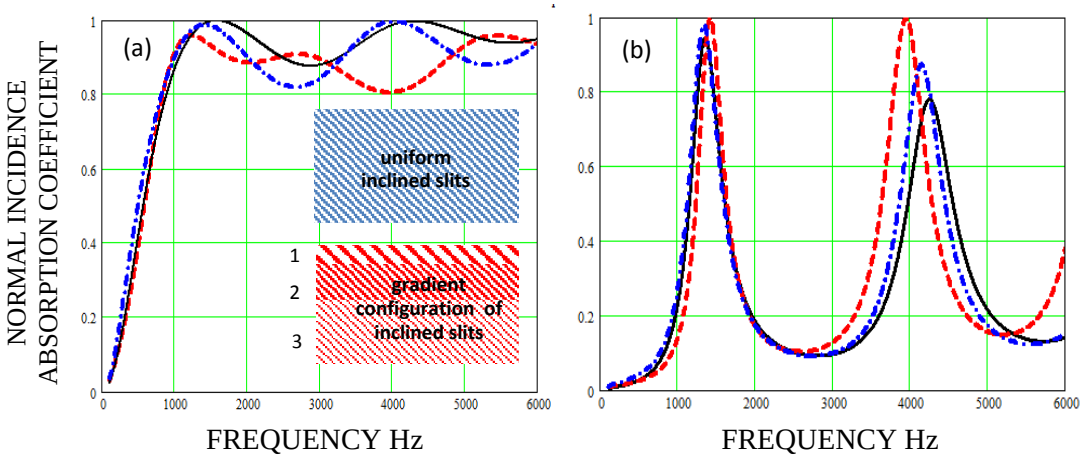


**Figure 1** Absorption coefficient spectra (solid black lines) predicted using the JCAL and JCA models respectively for hard-backed layers of (a) 57 mm thick melamine foam and (b) 26.4 mm thick perforated aluminium foam with the parameter values listed in Table 2. Dash-dot blue lines are predictions for (a) 45 mm thick and (b) 25 mm thick layers with identical inclined slits (40°and 65°). Broken red lines are predictions for (a) 30 mm thick and (b) 45 mm thick graduated inclined slit pore systems composed of three sublayers with the slit widths and inclinations listed in Table 3.

The high porosity (0.99) of the melamine foam means that the solid strips separating 0.18 mm wide inclined slits in the surface sub-layer of the 30 mm thick gradient system with the same porosity are only 1.8 microns wide. Moreover, the width of the solid strip between the 0.1 mm wide inclined slits in the third sub layer of the graduated system is only 1 micron. Accurate manufacture of sufficiently robust materials with such small dimensions poses a significant challenge. On the other hand, the rather lower porosity of the aluminium foam means that comparable absorption is achievable from simple slit microstructures in which the widths of slits and separating solid strips are on the order of mm, therefore feasible using current 3D printing technology.

## 2.3 Periodically non-uniform slits

The tortuosity due to inclined pores (equation (4)) results from a straightforward geometrical interpretation of tortuosity as the square of the ratio between pore length and sample length. But a more general interpretation depends on the length of the fluid streamlines. The acoustical properties resulting from pores composed from $n$ adjoining cylinders with area $A_n$ and length $l_n$ have been considered [8,18,19]. The non-uniformity of the pore cross section perturbs the fluid streamlines so that the tortuosity is larger than 1 even when the pores are normal to the surface. If the pressure gradient and velocity are assumed to be uniform in each section, thereby

ignoring the complicated micro-velocity fields associated with the abrupt changes in cross section, then the tortuosity is given approximately by [18]

$$T = \frac{\sum A_n l_n}{(\sum l_n)^2} \sum \frac{l_n}{A_n} \tag{11}$$

This leads to an expression for the tortuosity of a two-diameter cylindrical pore structure [8,18]

$$T = \frac{(l_1 A_2 + l_2 A_1)(l_1 A_1 + l_2 A_2)}{(l_1 + l_2)^2 A_1 A_2}. \tag{12}$$

Consider identical slit-like pores with alternating widths of the form shown in Figure 2(a), with narrower slit sections providing the surface porosity. The pore axes are normal to the surface of a hard-backed layer of thickness $d$. For this arrangement, $A_1 = 2b$, $A_2 = 2b(1+\delta)$, $l_2 = \varepsilon l_1$, hence

$$T(\varepsilon, \delta) = 1 + \frac{\varepsilon \delta^2}{(1+\varepsilon)^2 (1+\delta)} \tag{13a}$$

Figure 2(b) shows how the tortuosity given by (13a) is predicted to vary with the wider section width ($2b$ ($1+\delta$)). Fig. 2(c) shows the predicted variation in tortuosity with the ratio of section lengths ($\varepsilon$) when $b$ = 0.001 m and the larger section width is 0.006 m i.e. three times that of the narrower section ($\delta$ = 2).

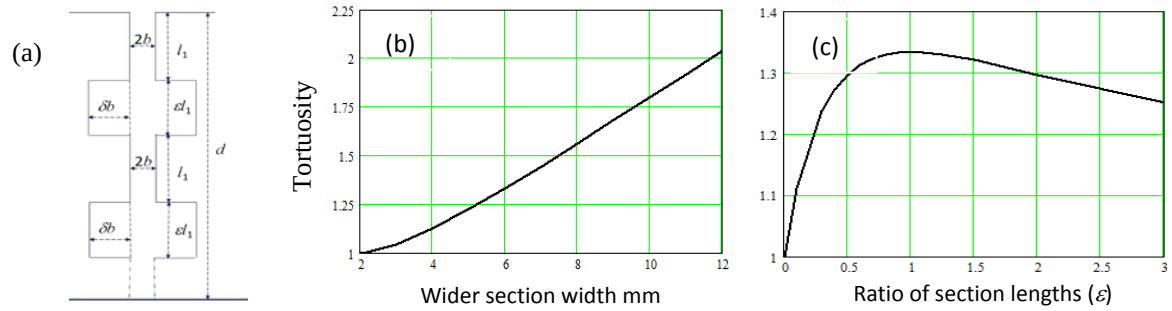


**Figure 2** (a) a periodically non-uniform slit; (b) and (c) predicted variations of tortuosity with the dimensions of the non-uniformity using eqn. (13a).

Tortuosity due to non-uniformity is maximum when the section lengths are equal ($\varepsilon = 1$). In this case, for non-uniform slits either normal or inclined to the surface from (13a) and (4),

$$T(1, \delta) = 1 + \frac{\delta^2}{4(1+\delta)}, T(1, \delta, \theta) = \left(1 + \frac{\delta^2}{4(1+\delta)}\right) / cos^2(\theta) \tag{13b,c}$$

The complex density in a non-uniform pore with $n$ sections of area $A_n$ and length $l_n$ may be written [18]

$$\rho(\omega) = T(\varepsilon, \delta) \frac{\sum_n \rho_n(\omega) l_n / A_n}{\sum_n l_n / A_n} \tag{14a}$$

where $\rho_n(\omega)$, $l_n$ and $A_n$ are the complex density, length and cross sectional area in the n$^{th}$ section respectively.

The acoustical properties of a system of parallel identical non-uniform pores composed from $n$ adjoining cylinders with a distribution of areas $A_n$ but equal section lengths ($l_n$) have been considered [20], but the expression given for complex density, viz.

$$\rho(\omega) = \frac{\sum_n \rho_n(\omega) / A_n}{\sum_n (1/A_n)}, \tag{14b}$$

appears not to include tortuosity associated with non-uniformity since, from (11), after allowing for equal section lengths, the tortuosity due to non-uniformity is,

$$T = \sum A_n \sum 1/A_n. \quad (14c)$$

With $n$ = 1,2; $A_1 = 2b$, $A_2 = 2b(1+\delta)$ and $l_2 = \varepsilon l_1$, (14a) becomes

$$\rho(\omega) = T(\varepsilon, \delta)\frac{(1+\delta)\rho_1(\omega)+\varepsilon\rho_2(\omega)}{1+\delta+\varepsilon} \quad (15)$$

If the pores are non-uniform slits, then from (1) and (2),

$$\rho_{1,2}(\omega) = \rho_0 \Big/ \left[1 - \frac{\tanh\left(\lambda_{1,2}\sqrt{(-i)}\right)}{\lambda_{1,2}\sqrt{(-i)}}\right],\ \lambda_1 = b(\omega/v), \lambda_2 = b(1+\delta)(\omega/v). \quad (16)$$

The complex compressibility in a non-uniform pore with $n$ sections may be written [16],

$$C(\omega) = \frac{\sum_n C_n(\omega) A_n l_n}{\sum_n A_n l_n} \quad (17)$$

For a staggered array of periodically non-uniform slits (Fig.2(a)), this becomes

$$C(\omega) = \frac{C_1(\omega)+\varepsilon(1+\delta)C_2(\omega)}{1+\epsilon(1+\delta)} \quad (18)$$

Note that (16) and (18) are independent of the section length ($l_1$). The staggered arrangement ensures that the surface porosity is the same as the bulk porosity which is $\left(1+\frac{\delta}{2}\right)/(1+\delta)$.

Figure 3 compares absorption coefficient spectra predicted for 30 mm thick hard-backed layers of porosity 0.6 corresponding to either uniform slit pores of width 1 mm (broken lines) or staggered non-uniform slit pores (continuous lines) with $b$ = 0.5 mm and $\delta$ = 4, which implies that the wide section width is 5 mm, (a) parallel to and (b) inclined at 70° to the surface normal. The increase in tortuosity due to pore non-uniformity is predicted to lower the quarter wavelength resonance frequency. Inclining non-uniform slits is predicted to lower the frequency of the resonance further but to increase both the amplitude and the Q-factor of the resonance.

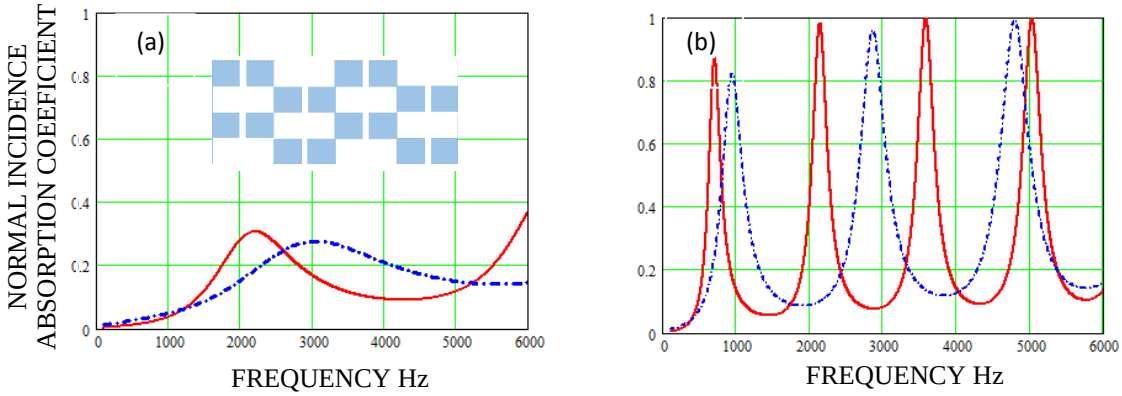


**Figure 3** Absorption coefficient spectra predicted for a 0.03 m thick hard-backed layer with porosity 0.6 containing uniform 1 mm wide slits (broken lines) separated by 0.67 mm compared with those predicted using (13) and (15) – (18) for staggered non-uniform pores with 1 mm wide narrow sections and 5 mm wide wider sections ($\delta$ = 4) of the same length ($\varepsilon$ = 1) (continuous lines): (a) parallel to the surface normal (b) inclined at 70° to the surface normal.

The sound absorption of a dual-porosity arrangement involving two different widths of orthogonal intersecting uniform slits has been considered previously [10]. Such an arrangement is predicted to result in low-Q quarter wavelength layer resonance. The quarter wavelength layer resonance frequency is predicted to be lowered if non-uniform and dual slit arrangements are combined. Figures 4(a) and (b) compare predictions for a system of meso- and micro-slits, in which the meso-slits are either uniform or have alternating slit widths (Fig. 2(a)).

According to Fig. 4(a) the predicted result of non-uniform meso-slits, normal to the surface, is not only to lower the frequency of the quarter-wavelength layer resonance but also increase its magnitude compared with uniform meso- and micro- slits [10]. Fig. 4(b) shows that, if the slits are inclined at 70° to the surface normal, then making the meso-slits non-uniform, is predicted to lower the frequency of the quarter-wavelength layer resonance still further but reduce its magnitude compared with that predicted for similarly inclined uniform meso- and micro-slits.

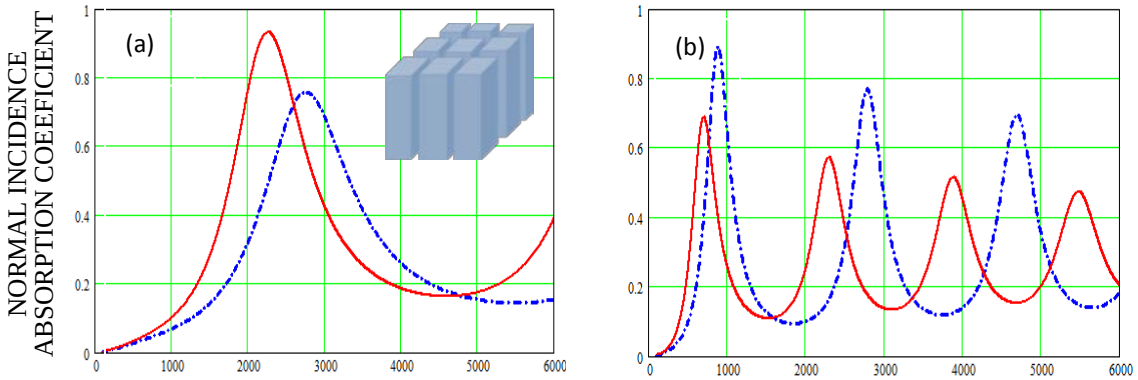


**Figure 4** Absorption coefficient spectra predicted for a 30 mm thick hard-backed layer, porosity 0.3, containing uniform 2 mm wide meso-slits and 0.2 mm wide micro-slits (broken blue lines) compared with those predicted for meso-slits with alternating 10 mm and 2 mm wide sections and 0.2 mm wide micro-slits (continuous red lines) (a) parallel to and (b) inclined at 70° to the surface normal.

# 3 PARTITION EFFECTS

## 3.1 Partitions with gaps

The low frequency absorption of a hard-backed rigid-porous layer can be improved by inserting regularly-spaced rigid partitions [3,4]. At frequencies below the onset of scattering within the material, i.e. when the incident wavelengths are larger than the partition period and layer thickness, the impedance of the porous layer is increased by a factor of the centre-to-centre spacing of the partitions divided by their width at the surface [3].

*d*

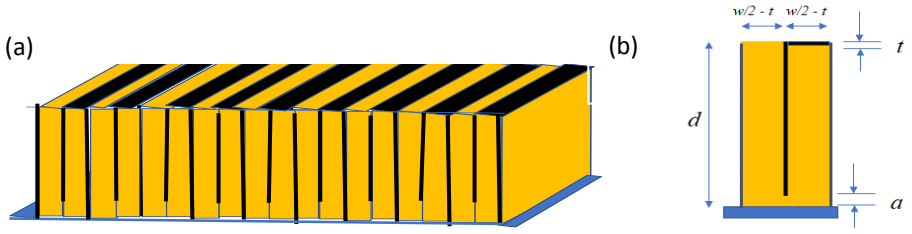


**Figure 5** (a) An arrangement of partitioned cells in a hard-backed layer of porous material (b) single cell divided by a vertical partition with gap

Figure 5(a) shows a periodic arrangement of partitions in a hard-backed layer of porous material, in which alternate vertical partitions have gaps. Figure 5(b) shows a single cell of this arrangement. The central vertical partition of thickness $t$ (< $w$/2) has a gap, width $a$, at the bottom. The left-hand portion of the cell with width $w/2 - t$ has an 'open' top but the top of the right-hand portion is 'closed' by a rigid horizontal partition of thickness $t$ and width $w$/2. This arrangement increases the surface impedance of the unpartitioned layer by a factor of 2.

After using an effective medium approach and regarding the gap beneath the central partition as the neck of a Helmholtz resonator consisting of the absorbing volume in the right-hand half of the cell [3], the surface impedance is given by equations (19a) and (19b).

$$Z_{AB} = Z_A \left[\frac{Z_B \cot(k_1 d) - iZ_A}{-iZ_B + Z_A \cot(k_1 d)}\right] \quad (19a)$$

where

$$Z_A = \frac{Z_1}{\eta}, Z_B = \frac{-i}{\eta}\left(\frac{\omega m}{\rho_0 c_0} - Z_1 \cot\left(k_1(d-t)\right)\right), m = (t + 2\delta a)\,\rho_1 w/2a, \quad (19b)$$

$Z_1$ , $k_1$ and $\rho_1$ being the characteristic impedance, propagation constant and complex density of the porous medium, $\eta = \left(\frac{w}{2} - t\right)/w$, $\delta = 1.9$, $m$ is the acoustic mass of the gap considered as a Helmholtz resonator and $Z_B$ is the associated impedance.

The partition configuration shown in Fig. 6(a) and its inset, may be considered to have two components (Fig. 6(b)); one is similar that shown in Figure 5(b) but with a smaller effective length and the other is a hard-backed porous layer of thickness $d' < d$. The reduction in surface porosity due to the presence of partitions is smaller than for the Fig. 5(b) configuration, but the different effective layer depths contribute resonances at intermediate frequencies, thereby potentially improving the overall absorption spectrum.

Using an effective medium approximation, the overall impedance of the cell type in Fig. 6(a) is given by parallel connection of the impedances of two sub-cells (Fig. 6(b)) i.e.

$$(Z_{CD})^{-1} = (Z_C)^{-1} + (Z_D)^{-1} \quad (20)$$

where $Z_C$ is given by equation (19), $(d - t)$ is replaced by $(d - d' - t)$ and $Z_D = Z_1 \cot(k_1 d')$.

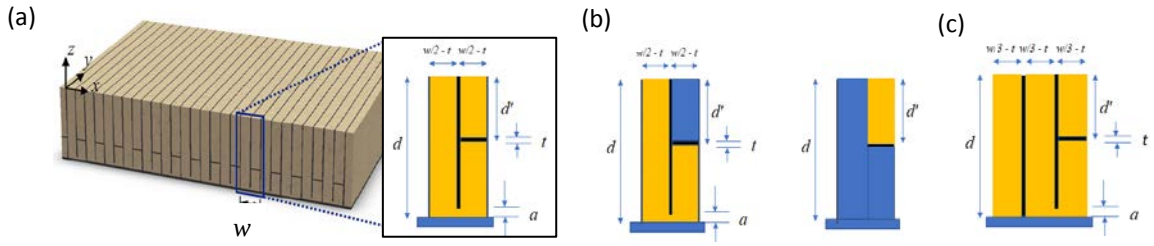


**Figure 6** (a) A partition configuration and inset with alternating hard-backed layer depths connected by a gap (b) hypothetical components of this cell type and (c) the configuration in (a) with an added hard-backed layer sub-cell.

Figure 6(c) shows a sub-cell in which a hard-backed layer of the same width as the others added to the Fig. 6(b) arrangement but without any connection to the neighbouring sub-cell. This increases the period of the vertical partitioning but adds another depth layer resonance. Again, using the effective medium approximation, the overall impedance is calculated from the impedance of hard-backed porous layer section of thickness $d$ (from equation (7) in parallel with that of the unit cell shown in Fig. 6(b) (from equations (19) and (20)).

Yang *et al* [3] assume that the porous medium hosting the partitions is representative of a porous metallic foam [5] and calculate its acoustical properties according to the JCA model with porosity 0.95, tortuosity 1.42, viscous characteristic length 0.18 mm, thermal characteristic length 0.36 mm and flow resistivity 8.9 kPa s m$^{-2}$.

Absorption coefficient spectra predictions for partitioned 30 mm thick hard-backed layers are compared in Fig.7. In Fig. 7(a), the solid black curve represents the prediction for a metallic foam using the JCA parameters assumed by Yang et al [3]. Instead of the placing the partitions in such a metallic foam, they are assumed to be embedded (see sketch on Figure) in an array of 0.2 mm wide identical parallel uniform slits inclined at 30$^o$ to the surface normal (tortuosity 4/3, porosity 0.95, flow resistivity 7.7 kPa s m$^{-2}$). The absorption coefficient for the unpartitioned slit array is represented by the broken blue line. The dash-dot red curve represents

the prediction for arrangement with partitioned cell width ($w$) of 10 mm, gap ($a$) of 1 mm, and a partition thickness ($t$) of 0.5 mm. While the unpartitioned slit array is predicted to offer better overall absorption than the metallic foam, the partitioned slits are predicted to offer superior absorption below 3.5 kHz but more oscillatory absorption above this frequency.

In Fig. 7(b), the broken and solid black lines represent predictions for unpartitioned 0.2 mm wide slits inclined at 45º (tortuosity 2, flow resistivity 11.5 kPa s $m^{-2}$) and 60º (tortuosity 4, flow resistivity 23 kPa s $m^{-2}$) to the surface normal respectively. The broken red and dash-dot blue curves represents the predictions with the partition cell arrangement shown in Fig. 6(a) and the sketch on the Figure ($d'$= 0.021 m, $w$, $a$ and $t$ as before) with slits are inclined at 45º and 60º respectively. As expected, while simply increasing the slit inclination in the unpartitioned slit arrays is predicted to improve the low frequency absorption, the partitions are predicted to smooth out the resulting oscillations in the spectra.

The absorption spectra in Fig. 7(c) represent predictions for cells partitioned as shown in Fig. 6(c) and the sketch on the Figure, with $d'$ = 0.022 m, $w$, $a$ and $t$ as before (sub-cell widths are $w$/3), for three angles of inclination of the slits (30º (broken red line); 45º (broken blue line), and 60º (dash-dot brown line)). With the stated parameters, the Fig.6(c) configuration appears to offer relatively little advantage. Nevertheless, compared with the Fig. 6(a) configuration, the additional resonance from the hard-backed sub-cell improves the predicted absorption between 2 and 3 kHz when the slits are inclined at 60º.

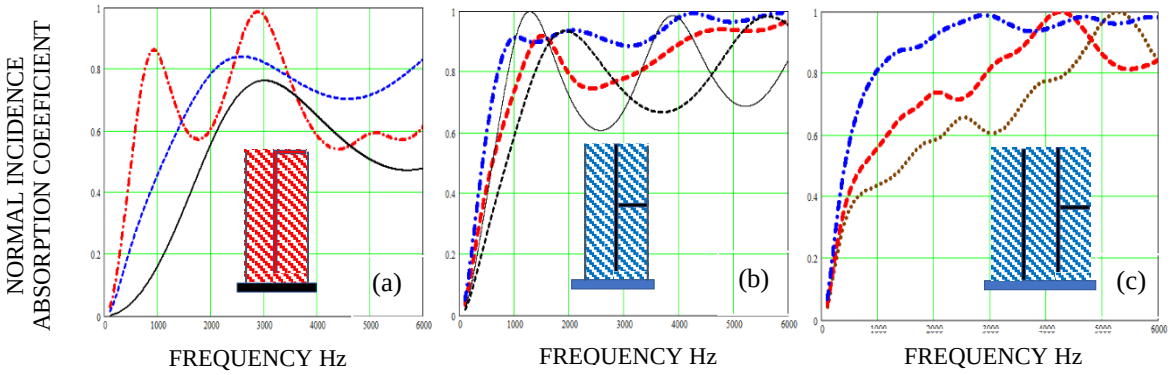


**Figure 7** (a) Predicted absorption coefficient spectra for a 3 cm thick hard-backed layers of metallic foam (continuous black line), unpartitioned 0.2 mm wide slits inclined at 30° (broken blue line) and inclined slits partitioned as in Fig.5 (dash-dot red line) (parameters in text) (b) unpartitioned slits or partitioned as in Fig.6(a) either normal to the surface (broken black and blue lines respectively) or inclined at 60° to the surface normal (continuous black and dash-dot blue lines respectively) (c) 0.2 mm wide slits inclined at 30°, 45° and 60° respectively partitioned as in Fig.6(c).

## 3.2 Horizontal partitions with varying lengths

The insertion of horizontal partitions with different lengths at different depths as well as vertical 'cell dividers' (see Fig. 8(a)), can be considered to create an array of side branch resonators within the host porous medium. The presence of rigid partitions in the surface reduces the surface porosity by more than the cell designs shown in Figs. 6. Yang *et al* [4] have investigated cell configurations containing up to eight partitions with surface partition width 18 mm, partition thickness 0.2 mm and a cell width of 30 mm equal to the layer depth i.e. more than 50% of the surface is rigid. They assume the porous material hosting the partitions to be representative of a porous metallic fibre [21], and calculate its acoustical properties using the JCA model with porosity 0.96, tortuosity 1.07, viscous characteristic length 0.273 mm, thermal characteristic length 0.672 mm and flow resistivity 2.843 kPa s $m^{-2}$.

The acoustical properties of a configuration involving $n$ horizontal partitions are predicted by using an effective medium approximation for each sub-layer formed between the partitions. The complex density and complex compressibility in the n$^{th}$ horizontal sub-layer are [4]

$$\rho_{b,n}(\omega) = \frac{\rho_b(\omega)}{1-\emptyset_n},\ \emptyset_n = \frac{l_n + l_{n-1} + (n-1)(d/n)}{2w},$$

$$C_n(\omega) = C(\omega)(1-\emptyset_n)\left[1 + \varphi\left\{\frac{\tan(k(\omega)(1-\emptyset_n)w)}{k(\omega)(1-\emptyset_n)w}\right\}\right],\ n = 1,2\ldots \quad (21)$$

where $\emptyset_n$ is the ratio of half the sum of adjacent horizontal partition lengths to the cell width and $\varphi = 1 - nt/d$ is the fractional volume of porous material in each effective sub-layer in the vertical direction. The surface impedance of the partitioned system is calculated using an appropriately modified form of equation (19).

As the host medium, instead of a metallic fibre material, consider an array of parallel uniform slits 0.28 mm wide, either normal to the surface or inclined and with edge-to-edge spacing 0.012 mm, corresponding to a flow resistivity of 2.9 kPa s m$^{-2}$.

The unit cell configuration shown in Figure 8(b) is assumed with three horizontal partitions of thickness 0.2 mm equally-spaced by a third of the overall layer depth. The surface partition width ($l_1$) is 2.7 mm, the partition edge slope angle $\theta$ is 30° and the cell width ($w$) is 20 mm. Less than 10% of the surface is rigid.

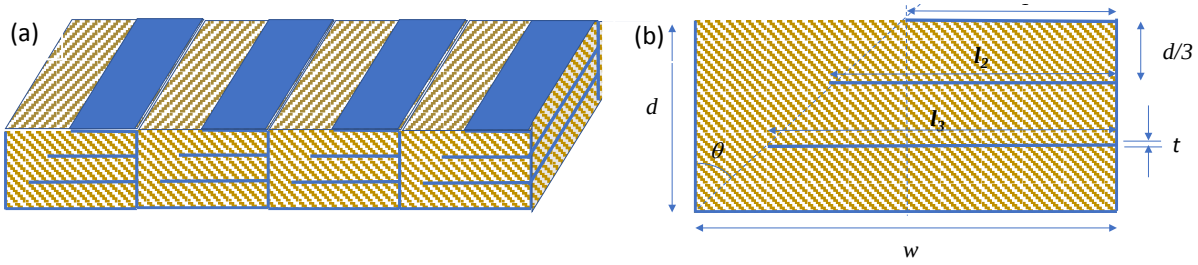


**Figure 8** (a) A porous layer of thickness $d$ with vertical partitions between contiguous cells and horizonal partitions at different depths within each cell (b) a cell of width $w$ with horizontal partitions spaced at $d$/3 and with edge slope angle $\theta$ of 30°

Figure 9 compares predicted absorption spectra for the 0.03 m thick hard-backed layers of metallic fibre (according to the previously stated JCA model parameters, continuous black line) and arrays of 0.28 mm wide slits without and with the partition arrangements shown in Fig.8. The broken black line represents the prediction for unpartitioned parallel identical uniform slits inclined at 45º. The continuous and broken (red) lines represent the predicted absorption spectra for partitioned slits normal to the surface and inclined at 45º respectively.

FEM simulations by Yang *et al* [4] have shown that the effective medium approximations become invalid at higher frequencies so predictions for the horizontal partition arrangements using (21) are limited to an upper frequency of 4 kHz. The first and second peaks in the predicted absorption spectrum for the partitioned material with inclined slits (broken red line) correspond to quarter and three-quarter wavelength layer resonances. The FEM simulations of the profiles of particle velocity by Yang *et al* [4] predict that, at these frequencies, the horizontal motion between the partitions is small whereas the third peak near 3.3 kHz and higher frequency peaks (not shown) involve resonances in both vertical and horizontal directions.

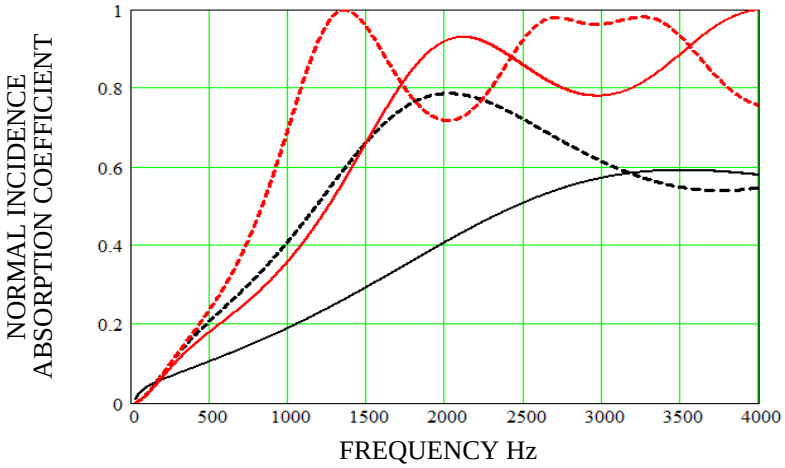


**Figure 9** Normal incidence absorption coefficient spectrum predicted for a metallic fibre material [4] (solid black line) and spectra predicted for an unpartitioned array of 0.28 mm wide slits inclined at 45° (broken black line) and for partitioned systems (Figure 9(a)) with slits either normal to the surface (solid red line) or inclined at 45° (broken red line)

According to Yang *et al* [4], the effective sub-layers between the horizontal partitions and between the longest partition and the cell base have different (slow) wave speeds. The side branch resonances introduced to the unpartitioned portion of each cell cause the real part of the effective bulk moduli in the sub-layers to become negative above a certain frequency. Figures 10(a) and (b) show predictions of frequency-dependent effective sound speeds and real parts of bulk moduli for the configuration shown in Fig. 8 with a partition edge slope of 30°.

Fig.10(b) shows that negative real parts of bulk moduli are predicted in the middle sub-layer at frequencies above 3.6 kHz and in the lowest sub-layer at frequencies above 2.3 kHz. Fig.10(a) shows that as well as the expected strong decrease of sound speed with depth, negative dispersion is predicted in the lowest sub-layer above 1 kHz.

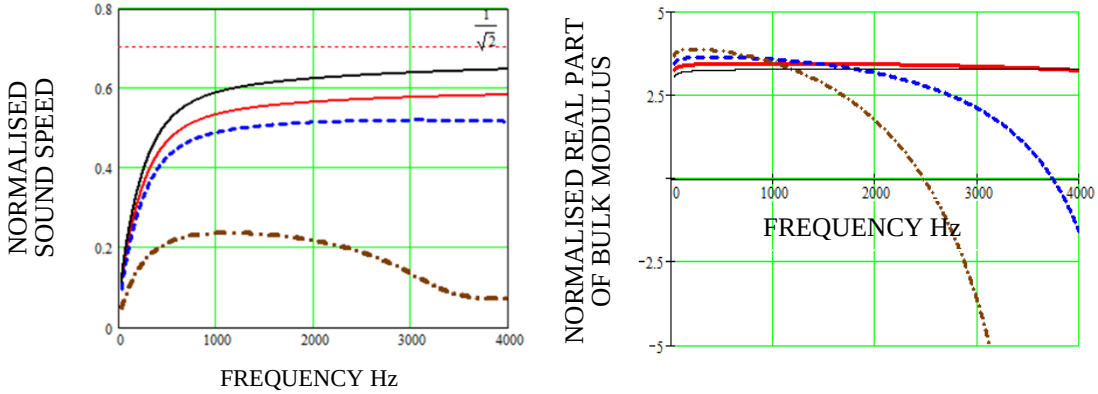


**Figure 10** (a) Predicted normalized sound speeds in (unpartitioned) 0.28 mm wide slits inclined at 45 (solid black line) and in each 'sub-layer' between the horizontal partitions shown in Fig. 9(b) (red, broken blue and broken brown respectively). Also shown is the high frequency limit (dotted red line) (b) Predicted real part of the normalised bulk modulus in an unpartitioned medium with 0.28 mm wide slits inclined at 45° to the surface normal (solid black line) and in each 'sub-layer' (Figure 9 (b)) (continuous red, broken blue and dash-dot brown lines respectively)

Figure 11 shows the predicted influence of the partition edge slope angle, $\theta$. Absorption spectra are predicted for slopes of 33° (broken black line; $l_1$ = 0.0005 m), 20° (dash-dot blue line; $l_1$ = 0.0091 m) and 10° (continuous red line; $l_1$ = 0.015 m). In accordance with other predictions (see Fig.6(b) in Yang *et* al [4]), decreasing the partition edge slope angle, $\theta$, is predicted to

reduce the frequency of the quarter wavelength layer resonance at the cost of reduced absorption coefficient values at higher frequencies. However, as noted above, the effective medium approximation used for the predictions is less accurate near 4 kHz.

The predicted absorption spectra given by the broken red line in Fig.9 and the dash-dot blue and broken black lines in Fig. 11 assume only three horizontal partitions (Fig. 8) but, nevertheless, are comparable with those predicted for the same thickness of a host porous medium having the previously-specified JCA parameters and between four and eight horizontal partitions with a partition edge slope of 20° [4].

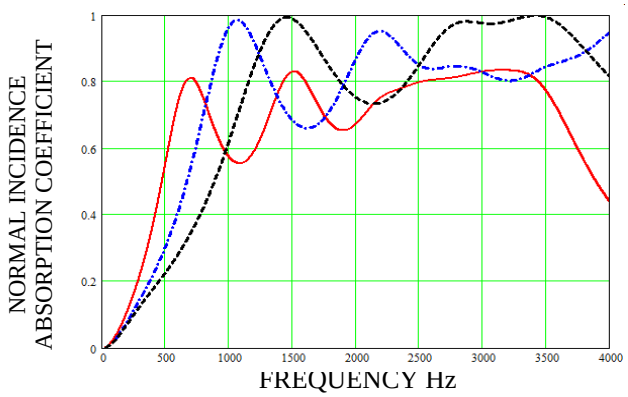


**Figure 11** Predicted influence of horizontal partition edge slope (33° (broken black line), 20° (dash-dot blue line) and 10° (continuous red line)) on absorption spectra associated with 3 cm thick hard-backed partitioned inclined slit configurations other dimensions as for Fig. 10.

## 4 CONCLUDING REMARKS

While the smaller slit dimensions and edge-to-edge spacings that have been considered are beyond current capabilities in additive manufacturing, they might become feasible in the future. Inevitably, departures from the proposed idealized designs will be introduced during manufacture, such as unequal slit dimensions or cross-sectional irregularities. But, for example, a sinusoidal variation in cross section increases tortuosity in a predictable way and predictions may be made for a known distribution in pore widths [10,20].

Although the predicted acoustical characteristics of a hard-backed array of vertical slits have been validated by experiments [21], the horizontal confinement of inclined slits that will occur in practice and, in any case, if partitions are introduced, may require interconnections between slits to realise the assumed effective medium properties. Further work is needed to investigate the extent and form of interconnections required and to model their effects.

Many aspects of porous absorber designs at macro- and micro-scales remain to be investigated. For the parameters used here and in Yang *et a*l [3] the predicted resonator effect due to the partitioning systems shown in Figs. 5 and 6 is small. It might be interesting to ascertain the circumstances for which this resonator effect would be larger and exploitable. There is scope for investigating other partition arrangements. Combinations of the unit cell configurations shown in Fig. 9 with different $d'$values [4] could be considered.

The combination of partition macrostructures with inclined slit microstructures has been considered here but combinations with other types of pore structures could be considered. It might be possible to construct thin porous layers that combine increased tortuosity and effective compressibility simultaneously, thereby offering even more scope for designing pore structures to achieve targeted acoustical performances.

**Acknowledgement**

The idea for this paper was initiated by activities and communications associated with the EC COST network DENORMS.

# 5 REFERENCES

[1] F Chevillotte, C, Perrot, R. Panneton, Microstructure based model for sound absorption predictions of perforated closed-cell metallic foams. J. Acoust. Soc. Am. **128** 1766 –76 (2010)
[2] H. Meng, S W Ren, F X Xin, *et al*. Sound absorption coefficient optimization of gradient sintered metal fiber felts. Sci China Tech Sci, **59** 699−708 (2016),
[3] J. Yang, J. S. Lee and Y. Y. Kim, Metaporous layer to overcome the thickness constraint for broadband sound absorption, J. Appl. Phys. **117** 174903 (2015).
[4] J. Yang, J. S. Lee, and Y. Y. Kim, Multiple slow waves in metaporous layers for broadband sound absorption, *J. Phys. D: Appl. Phys.* **50** 015301 (2017).
[5] J-P. Groby, O. Dazel, A. Duclos, L. Boeckx and L. Kelders, Enhancing the absorption coefficient of a backed rigid frame porous layer by embedding circular periodic inclusions, J. Acoust. Soc. Am. **130** 3771 – 3780 (2011).
[6] B Nennig, Y Renou, J-P Groby, and Y Auregan, A mode matching approach for modeling two-dimensional porous grating with infinitely rigid or soft inclusions, J. Acoust. Soc. Am. 131 3841–3852 (2012)
[7] F. Chevillotte and C. Perrot, Effect of the three-dimensional microstructure on the sound absorption of foams: A parametric study, J. Acoust. Soc. Am. 142 1130 – 1140 (2017).
[8] J-F. Allard and N. Atalla *Propagation of sound in porous media* Wiley (2009)
[9] A. Duval, M-T Hong, C. Perrot, V. Marcel, G. Bonnet, Chemistry-process morphology control of porous microstructures: a bottom-up acoustic optimisation approach, SIA Conference “Light-Weighting and Acoustical Materials in Vehicles”, Compiègne (2013)
[10] K. Attenborough, Microstructures for lowering the quarter wavelength resonance frequency of a hard-backed rigid-porous layer, Applied Acoustics, **130** 188–194 (2018)
[11] P. Leclaire, O. Umnova, T. Dupont and R. Panneton, Acoustical properties of air-saturated porous material with periodically distributed dead-end pores. J. Acoust. Soc. Am. **134** 1772 – 1782 (2015)
[12] Z. Liu, J. Zhan, M. Fard and JL Davy Acoustic properties of a porous polycarbonate material produced by additive manufacturing, Materials Letters **181** 296 – 299 (2016)
[13] D. C. Akiwate, M. D. Date, B. Venkatesham, S. Suryakumar, Acoustic properties of additive manufactured narrow tube periodic structures. Applied Acoustics **136** 123 – 131 (2018)
[14] S. Guessasma, W. Zhang, J. Zhu *et al*, Challenges of additive manufacturing technologies from an optimisation perspective, Int. J. Simul. Multisci. Des. Optim. 6, A9 (2015)
[15] M. R. Stinson, The propagation of plane sound waves in narrow and wide circular tubes and generalisation to uniform tubes of arbitrary cross-sectional shape, J. Acoust. Soc. Am. **89** (1) 550-558, (1991)
[16] P. C. Carman, *Flow of gases through porous media*, Butterworths, London, 1953
[17] Zwikker C and Kosten CW. *Sound Absorbing Materials*. Elsevier. Amsterdam. 1949.
[18] M. R. Stinson and Y. Champoux, Propagation of sound and the assignment of shape factors in model porous materials having simple pore geometries, J. Acoust. Soc. Am. **91**, 685 – 695 (1992)
[19] Y. Champoux and M. R. Stinson, On acoustical models for sound propagation in rigid frame porous materials and the assignment of shape factors”, J. Acoust. Soc. Am. **92** 1120 – 1131 (1992)

[20] K. Horoshenkov, J-P. Groby and O Dazel, Asymptotic limits of some models for sound propagation in porous media and the assignment of the pore characteristic lengths, J. Acoust. Soc. Am. 139 1120 – 1131 (2016)
[21] J-P Groby, W Lauriks and T E Vigran, Total absorption peak by use of a rigid frame porous layer backed by a rigid multi irregularities grating J. Acoust. Soc. Am. **127** 2865–74 (2010)
[22] Imran Bashir, Shahram Taherzadeh, and Keith Attenborough, Surface waves over periodically-spaced strips. J. Acoust. Soc. Am. **134** (6) 4691 – 4697 (2013)